Estimation of temporal variations in the magnetic field arising from the motional induction that accompanies seismic waves at a large distance from the epicentre

Ken'ichi Yamazaki

Miyazaki Observatory, Research Center for Earthquake Prediction, Disaster Prevention Research Institute, Kyoto University, 3884, Kaeda, Miyazaki, Miyazaki 889–2161, Japan. Email: kenichi@rcep.dpri.kyoto-u.ac.jp

SUMMARY

Temporal variations in the electromagnetic field that accompany earthquakes are generated by various mechanisms, of which this study focuses on variations in the magnetic field arising from motionally induced electric currents that accompany seismic waves at large distances (several hundred kilometres) from the epicentre. A simple situation is considered in which seismic waves are approximated by plane waves and the electrical conductivity of the Earth's crust has a stratified structure. Solutions of Maxwell's equations corresponding to this situation have analytical expressions. Analysis of the solutions verifies that *SH* waves do not generate variations in the EM field above the ground surface, thereby implying that Rayleigh waves are dominant at a significant distance from earthquake epicentres. Numerical examples demonstrate that the amplitudes of the variations in the magnetic field monotonically increase with increasing conductivity, although attenuation because of the skin effect cannot be ignored. The amplitudes of the generated magnetic field can be sensitive to the conductivity of both the shallow and deep crust. Nevertheless, calculations assuming a simplified conductivity structure provide an upper limit to the possible amplitudes of variations in the magnetic field because of seismic waves. For example, the amplitudes of variations in the magnetic field arising from a Rayleigh wave with displacement amplitude of 10 cm and a period of 30 s are as large as 0.1 nT, close to the limit of detection under typical observation conditions. It is also suggested that phase differences between seismic ground motions and variations in the magnetic field are insignificantly influenced by details of conductivity structures, and they occur within a rather narrow range of values determined by the direction orientation of the ambient geomagnetic field. In the future, if a detection limit of 0.01 nT becomes available, phase difference may be used to distinguish variations arising from the motional induction, from variations arising from other mechanisms.

Key words: Electrical properties; Electromagnetic theory; Earthquake ground motions.

1 INTRODUCTION

Temporal variations in the electromagnetic (EM) field associated with seismic ground motions have been widely reported (e.g. Eleman 1965; Karakelian *et al*. 2002; Matsushima *et al*. 2002; Ujihara *et al*. 2004; Abdul Azeez *et al*. 2009; Honkura *et al*. 2009; Kuriki *et al*. 2011). Such variations are expected to arise because seismic waves can be converted to EM variations by numerous mechanisms, including the motional induction in the Earth's crust that accompanies seismic waves (e.g. Matsushima *et al*. 2002). This occurs because the Earth's crust has finite electrical conductivity and ground motions in the ambient geomagnetic field yield an electromotive force, resulting in motionally induced electric currents. Theoretical and experimental studies predict that other mechanisms

also act to convert seismic ground motions or stress changes into EM variations, including the electrokinetic effect (e.g. Ishido & Mizutani 1981; Jouniaux *et al*. 1994; Pride 1994; Bordes *et al*. 2006, 2008), the piezoelectric effect (e.g. Bishop 1981; Ghomshei & Templeton 1989; Huang 2002), the piezomagnetic effect (e.g. Nagata 1970; Stacey & Johnston 1972; Zlotnicki *et al*. 1981) and the ion-resonance effect (Honkura *et al*. 2009; Kuriki *et al*. 2011). The results of these studies indicate that seismic waves are generally accompanied by variations in the EM field.

Quantitative investigations are important because they can provide fundamental insight into the conversion of mechanical forces into EM variations. If EM variations larger than the sum of the contributions of known conversion mechanisms are observed at the time of earthquakes, they should be interpreted as consequences of

unknown conversion mechanisms in the Earth's crust or of disturbances in the Earth's external field.

In many previous studies, EM variations were estimated at sites located close to seismic sources. Formulations and calculations for this purpose have been developed corresponding to the electrokinetic effect (e.g. Haartsen & Pride 1997; Garambois & Dietrich 2002; Gao & Hu 2010), the motional induction (e.g. Gershenzon *et al*. 1993), the piezoelectric effect (Ogawa & Utada 2000a) and the piezomagnetic effect (e.g. Okubo *et al*. 2011). It is reasonable to focus on relatively small distances from epicentres because observations are usually obtained at ranges of less than several tens of kilometres (e.g. Honkura *et al*. 2002, 2004, 2009; Karakelian *et al*. 2002; Matsushima *et al*. 2002; Ujihara *et al*. 2004; Kuriki *et al*. 2011; Okubo *et al*. 2011).

Several studies have reported observations of EM variations during seismic events, both near the epicentre and at a distance of more than several hundreds of kilometres (Eleman 1965; Abdul Azeez *et al*. 2009; Taira *et al*. 2009). In principle, theoretical calculations of EM phenomena near the epicentre are also valid at locations far from the epicentre. Nevertheless, there are some advantages in considering only distant locations. For example, seismic waves can be approximated there by plane waves, whereas they should be treated as spherical waves at locations near the epicentre. An approximation by plane waves enables analytical or semi-analytical expressions of the EM variations arising from the piezoelectric effect (Ogawa & Utada 2000b) and the piezomagnetic effect (Yamazaki 2011a,b). Further studies are required to enable quantitative comparisons between observation and theory.

This paper considers EM variations arising from the motional induction that accompanies seismic plane waves. The situation considered in this analysis is summarized in Fig. 1. The remainder of this paper is organized as follows. In Section 2, the governing equations and assumptions are described for the problem of interest. In Section 3, a set of analytical solutions to the problem is derived,
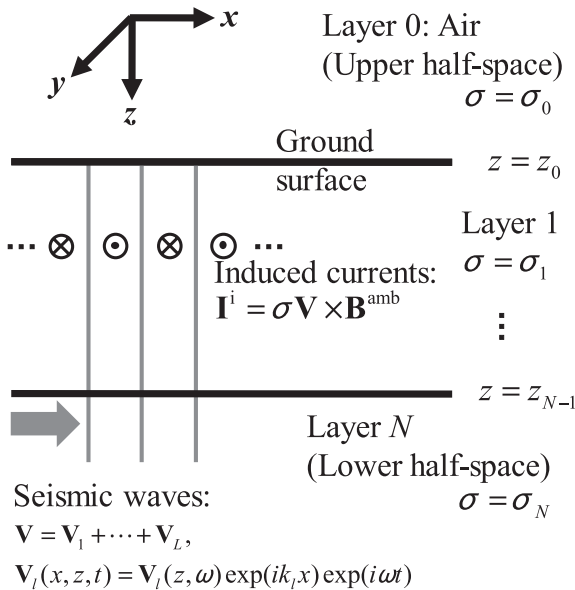
Figure 1. Configuration of the problem. The *x*-axis indicates the propagation direction of seismic waves in the horizontal plane; the *z*-axis is vertically downwards; and the *y*-axis is chosen in such a way that *xyz* forms a right-hand side orthogonal system. In this figure, σ represents conductivity, **V** represents the ground velocity, $\mathbf{B}^{\mathrm{amb}}$ represents the ambient geomagnetic field, $\mathbf{I}^{\mathrm{i}}$ represents the induced current density and k and ω represent the wavenumber and the angular frequency of the seismic wave, respectively.

yielding the important finding that *SH* waves do not generate variations in the magnetic field. Numerical predictions of amplitudes and phases of the generated variations in the magnetic field are presented in Sections 4 and 5, respectively. Section 6 presents additional discussions on relevant topics. Finally, the main conclusions are presented in Section 7.

2 GOVERNING EQUATIONS

This paper considers the conversion from seismic waves to EM variations in the frequency domain. Results in the time domain can be obtained by applying an inverse Fourier transform. Note, however, only a narrow band centred on the dominant frequency of seismic waves needs to be considered for estimating the amplitude of variations in the magnetic field, unless we want to determine an accurate time-series of EM variations (Yamazaki 2011a). Below, a time dependency of $\exp(-i\omega t)$, where ω represents the angular frequency, is assumed, following the convention in seismology (e.g. Aki & Richards 2002). Temporal variations in electric and magnetic fields (**E** and **B**, respectively) at the location $\mathbf{x} = (x, y, z)$ satisfy the following Maxwell's equations:

$$\nabla \cdot \varepsilon \mathbf{E}(\mathbf{x}, \omega) = \rho(\mathbf{x}, \omega), \tag{1}$$

$$\nabla \cdot \mathbf{B}(\mathbf{x}, \omega) = 0, \tag{2}$$

$$\nabla \times \frac{1}{\mu} \mathbf{B}(\mathbf{x}, \omega) + i\varepsilon\omega \mathbf{E}(\mathbf{x}, \omega) = \mathbf{I}(\mathbf{x}, \omega), \tag{3}$$

and

$$\nabla \times \mathbf{E}(\mathbf{x}, \omega) - i\omega \mathbf{B}(\mathbf{x}, \omega) = \mathbf{0}, \tag{4}$$

where ε and μ are the electric and magnetic permeabilities, respectively; **I** represents the current density; and ρ is the electric charge density. The current density is divided into two parts:

$$\mathbf{I}(\mathbf{x}, \omega) = \mathbf{I}^{\mathrm{c}}(\mathbf{x}, \omega) + \mathbf{I}^{\mathrm{i}}(\mathbf{x}, \omega), \tag{5}$$

where $\mathbf{I}^{\mathrm{c}}$ is a conductive current obeying Ohm's law, and $\mathbf{I}^{\mathrm{i}}$ is the induced current generated by ground motions. These terms are expressed by

$$\mathbf{I}^{\mathrm{c}}(\mathbf{x}, \omega) = \sigma(\mathbf{x})\mathbf{E}(\mathbf{x}, \omega) \tag{6}$$

and

$$\mathbf{I}^{\mathrm{i}}(\mathbf{x}, \omega) = \sigma(\mathbf{x})\mathbf{V}(\mathbf{x}, \omega) \times \mathbf{B}^{\mathrm{amb}}, \tag{7}$$

respectively, where **V** is the ground velocity and $\mathbf{B}^{\mathrm{amb}}$ represents the ambient geomagnetic field. This analysis considers time and spatial scales up to several minutes and several hundred kilometres, respectively. Although $\mathbf{B}^{\mathrm{amb}}$ varies over these scales, the amplitudes of these spatio-temporal variations are significantly smaller than the spatio-temporal average. Therefore, spatio-temporal variations in $\mathbf{B}^{\mathrm{amb}}$ should cause only minor changes on the resultant EM variations. For this reason, in the following discussion $\mathbf{B}^{\mathrm{amb}}$ is treated as a constant over the area and period of interest.

The governing equations are reduced to simplified forms as follows. The electric permeability and magnetic permeability are fixed to their values in a vacuum: ε_0 and μ_0, respectively. Phenomena involving charge separations, such as the electrokinetic and piezoelectric effects, are not considered; consequently, the charge density in eq. (1) is set to zero. Only seismic waves that can be represented by superpositions of plane waves propagating in the positive *x* direction are considered. Therefore, particle motions of the ground (i.e. **V**) are independent of *y*. In addition, it is assumed that electrical

conductivity has a layered structure with N boundaries located at $z_0 < \cdots < z_{N-1}$ (Fig. 1). The conductivity in each layer is assumed to be uniform, as follows:

$$\sigma(\mathbf{x}) = \sigma(z) = \sigma_n, \quad (z_{n-1} < z < z_n, \, n = 0, \cdots, N), \quad (8)$$

where $z_{-1} = -\infty$ and $z_N = +\infty$. Under these assumptions, the induced current density $\mathbf{I}^i$ in each layer is independent of y, and therefore $\mathbf{E}$ and $\mathbf{B}$ are independent of y.

With the above simplifications, the governing equations are reduced to

$$\frac{1}{\mu_0} \nabla \times \mathbf{B}(x, z, \omega) - \sigma'_n \mathbf{E}(x, z, \omega) = \mathbf{I}^i(x, z, \omega) \quad (9)$$

and

$$\nabla \times \mathbf{E}(x, z, \omega) - i\omega \mathbf{B}(x, z, \omega) = 0, \quad (10)$$

where

$$\sigma'_n = \sigma_n - i\omega\varepsilon_0, \quad (11)$$

together with the conditions of eqs (1) and (2) with $\rho = 0$. When $\mathbf{V}$ and $\mathbf{B}^{\text{amb}}$ are known, $\mathbf{I}^i$ is determined by eq. (7). The object is to solve eqs (9) and (10) for a given $\mathbf{I}^i$ to determine $\mathbf{E}$ and $\mathbf{B}$.

Because phenomena are considered at a single frequency ω, it is sufficient to calculate $\mathbf{E}$ and $\mathbf{B}$ arising from an induced current distribution expressed by

$$\mathbf{I}^i(x, z, \omega) = \mathbf{I}^i(k_x, z, \omega) \exp(+ik_x x), \quad (12)$$

where k_x denotes the horizontal wavenumber, satisfying $k_x = \omega/v_x$ and v_x is the propagation velocity of the seismic wave with respect to the horizontal plane. Clearly, all field quantities depend on $\exp(+ik_x x)$ for this case. Consequently, the spatial derivative of $\partial/\partial x$ can be replaced by the factor ik_x in the horizontal Fourier wavenumber domain. Herein, the variables x, ω and k_x, which appear only as arguments of harmonic functions, are omitted for simplicity.

3 SOLUTIONS OF THE EQUATIONS

3.1 Explicit forms of solutions

Although we need to solve eqs (9) and (10) for a given $\mathbf{I}^i$ to determine $\mathbf{E}$ and $\mathbf{B}$, we can refer to a similar problem regarding the piezomagnetic effect (Yamazaki 2011a). Using those solutions, we can easily obtain the explicit forms of solutions of eqs (9) and (10), as follows.

In layer n (i.e. $z_{n-1} < z < z_n$), the z dependencies of $\mathbf{B}$ and $\mathbf{E}$ are expressed as

$$B_x(z) = \mu_0 \sigma'_n \int_{-\infty}^{+\infty} \left[-\frac{\partial}{\partial z} G_y(z, z') \right] I_y(z') \mathrm{d}z', \quad (13)$$

$$B_y(z) = \mu_0 \sigma'_n \int_{-\infty}^{+\infty} \left[\frac{\partial}{\partial z} G_x(z, z') I_x(z') \right. \\ \left. - ik_x G_z(z, z') I_z(z') \right] \mathrm{d}z', \quad (14)$$

$$B_z(z) = \mu_0 \sigma'_n \int_{-\infty}^{+\infty} ik_x G_y(z, z') I_y(z') \mathrm{d}z', \quad (15)$$

$$E_x(z) = \int_{-\infty}^{+\infty} [(i\omega\mu_0\sigma'_n - k_x^2)G_x(z, z')I_x(z') \\ + ik_x \frac{\partial}{\partial z} G_z(z, z')I_z(z')]\mathrm{d}z', \quad (16)$$

$$E_y(z) = \int_{-\infty}^{+\infty} i\omega\mu_0\sigma'_n G_y(z, z')I_y(z')\mathrm{d}z', \quad (17)$$

and

$$E_z(z) = \int_{-\infty}^{+\infty} [ik_x \frac{\partial}{\partial z} G_x(z, z')I_x(z') \\ + \left(i\omega\mu_0\sigma'_n + \frac{\partial^2}{\partial z^2} \right) G_z(z, z')I_z(z')]\mathrm{d}z', \quad (18)$$

where I_i ($i = x, y$ or z) is each component of $\mathbf{I}^i$, and G_i is the solution of

$$\left(-k_x^2 + \frac{\partial^2}{\partial z^2} + i\omega\sigma'_n \right) G_i(z, z') = -\frac{1}{\sigma'_n} \delta(z - z'), \quad (19)$$

where $\delta(\cdot)$ represents Dirac's delta function. Note that eq. (19) is equivalent to

$$\int_{-\infty}^{+\infty} \left(-k_x^2 + \frac{\partial^2}{\partial z^2} + i\omega\sigma'(z') \right) G_i(z, z')I_i(z')\mathrm{d}z' \\ = -\frac{1}{\sigma'_n} I_i(z), \quad (20)$$

for $z_{n-1} < z < z_n$, $0 \le n < N$; hence, G_i can be interpreted as a vector Green's function for dipole sources aligned in the y direction. We can easily confirm by direct substitution that eqs (13)–(18) with the x dependency of $\exp(ik_x x)$ satisfy eqs (9) and (10) for G_i defined by eq. (20). In all layers (i.e. $z_{n-1} < z < z_n$, $0 \le n \le N$), the solution of eq. (19) is expressed in the following form:

$$G_i(z, z') = U_i^{(n)}(z') \exp(+u_n z) + D_i^{(n)}(z') \exp(-u_n z) \\ + \delta_{n,m} \frac{1}{2u_n\sigma'_n} \exp(-u_n |z - z'|), \quad (21)$$

where m represents the layer to which z' belongs, $\delta_{n,m}$ is the Kronecker's delta, $U_i^{(n)}$ and $D_i^{(n)}$ are functions of z' and ω, and

$$u_n = (k_x^2 + i\omega\mu_0\sigma'_n)^{1/2}. \quad (22)$$

Because G_i should converge to a finite value at $|z - z'| \to \infty$, a condition of $\text{Re}(u_n) > 0$ should be imposed.

3.2 Constraint imposed by EM boundary conditions

The functions $U_i^{(n)}$ and $D_i^{(n)}$ are determined by the boundary conditions of the EM fields. For the top and bottom half-spaces (i.e. layers 0 and N), $U_i^{(n)}$ and $D_i^{(n)}$ should satisfy

$$U_i^{(N)}(z') = D_i^{(0)}(z') = 0, \quad (23)$$

because terms involving $U_i^{(n)}$ and $D_i^{(n)}$ represent variations propagating upwards and downwards, respectively, and there are no sources at positive or negative infinity. Conditions at other boundaries are the continuity of B_x, B_y, E_x and E_y at each boundary.

To obtain the conditions of $U_i^{(n)}$ and $D_i^{(n)}$, it is necessary to rewrite the boundary conditions on B_x, B_y, E_x and E_y to conditions on G_x, G_y and G_z. Because the boundary conditions must be satisfied for an arbitrary distribution of $\mathbf{I}^i$, we can choose simple conditions without loss of generality. For example, consider the case of $I_y = I_z = 0$.

The boundary conditions for B_y and E_x at $z = z_n$ ($0 < n < N$) then impose the following conditions on G_x:

$$\lim_{h \to +0} \sigma_n' \frac{\partial}{\partial z} G_x(z_n - h, z') = \lim_{h \to +0} \sigma_{n+1}' \frac{\partial}{\partial z} G_x(z_n + h, z') \qquad (24)$$

and

$$\lim_{h \to +0} (i\omega\mu_0\sigma_n' - k_x^2)G_x(z - h, z')$$
$$= \lim_{h \to +0} (i\omega\mu_0\sigma_{n+1}' - k_x^2) \times G_x(z + h, z'). \qquad (25)$$

These conditions, together with condition (23), completely determine $U_x^{(n)}$ and $D_x^{(n)}$ for $0 \le n \le N$ because now we have $2(N+1)$ linear equations in $2(N+1)$ unknowns. Similarly, the case of $I_x = I_z = 0$ yields the conditions of

$$\lim_{h \to +0} \sigma_n' \frac{\partial}{\partial z} G_y(z_n - h, z') = \lim_{h \to +0} \sigma_{n+1}' \frac{\partial}{\partial z} G_y(z_n + h, z') \qquad (26)$$

and

$$\lim_{h \to +0} \sigma_n' G_y(z_n - h, z') = \lim_{h \to +0} \sigma_{n+1}' G_y(z_n + h, z') \qquad (27)$$

imposed on G_y to determine $U_y^{(n)}$ and $D_y^{(n)}$, and the case of $I_x = I_y = 0$ yields the conditions

$$\lim_{h \to +0} \frac{\partial}{\partial z} G_z(z_n - h, z') = \lim_{h \to +0} \frac{\partial}{\partial z} G_z(z_{n+1} + h, z'), \qquad (28)$$

and

$$\lim_{h \to +0} \sigma_n' G_y(z_n - h, z') = \lim_{h \to +0} \sigma_{n+1}' G_y(z_{n+1} + h, z'), \qquad (29)$$

imposed on G_z to determine $U_z^{(n)}$ and $D_z^{(n)}$.

In practical terms, it is important to investigate properties of the EM field near the ground surface, $z = z_0$, because EM data are usually acquired at this level. The ground surface is in contact with the air layer. The conductivity of the air is approximated as zero. Because a condition of $\varepsilon_0\omega \ll \sigma_n$ ($n > 0$) is satisfied for the frequency of seismic waves, $\sigma_0' \ll \sigma_n'$ ($n > 0$) is also satisfied. Therefore, the EM field in layer 0 is determined by approximating $\sigma_0' \simeq 0$. Because the expression of the magnetic field (eqs 13–15) involves the factor σ_n', B_i in layer 0 becomes zero, unless any of G_i or $\partial G_i/\partial z$ becomes infinite when σ_0' approaches zero.

Concerning G_x, the boundary conditions (eqs 24 and 25) constitute a system of equations for $U_x^{(n)}$ and $D_x^{(n)}$, regardless of whether σ_0' is finite or zero. The determinant of the matrix defining these equations is not zero; consequently, $U_x^{(n)}$ and $D_x^{(n)}$ are finite according to Cramer's formula. Therefore, $\sigma_0'G_x$ becomes zero when $\sigma_0' = 0$. The same discussion applies to G_z: $\sigma_0'G_x$ is confirmed to be zero when $\sigma_0' = 0$. In contrast, the boundary conditions involving G_y do not yield $\sigma_0'G_y = 0$. When $\sigma_0' = 0$, the unknown $U_y^{(0)}$ disappears from eqs (26) and (27); hence, $U_y^{(0)}$ is indeterminable. Nevertheless, eqs (26) and (27) define a system of equations for $\sigma_n'U_y^{(n)}$ and $\sigma_n'D_y^{(n)}$, producing a finite value of $\sigma_0'U_y^{(0)}$. Therefore, $\sigma_0'G_y$ generally has a finite value, even when $\sigma_0' = 0$. Examples of explicit forms of $\sigma_n'U_y^{(n)}$ and $\sigma_n'D_y^{(n)}$ corresponding to two- and three-layer cases (i.e. $N = 1$ and 2, respectively) are presented in Appendix A.

On the basis of the above discussion, it is concluded that currents induced by *SH* waves of seismic waves do not generate variations in the magnetic field, for the following reason. When σ_0' is approximated by zero, $\sigma_0'G_x$ and $\sigma_0'G_z$ are negligible. Because G_x is an exponential function of z, $\sigma_0'\partial G_x/\partial z$ is also negligible. Therefore, B_y is also negligible (eq. 14). The expressions of B_x and B_z do not include terms involving I_x or I_z (eqs 13 and 15). Because $\mathbf{I}^i$ is the vector product of $\mathbf{V}$ and $\mathbf{B}^{amb}$, ground motions in the y direction do

not contribute to I_y, meaning $\mathbf{B}$ is independent of such ground motions. In the coordinate system employed here, seismic *SH* waves cause ground motions only in the y direction. Therefore, *SH* waves (including Love waves) do not generate variations in the magnetic field.

Taking into account the above discussion, the procedure employed to estimate variations in the EM field because of electric currents induced by seismic waves is summarized as follows. In the frequency domain of time, the velocity fields of the seismic plane waves are expressed in the form

$$\mathbf{V}(x', z') = \exp(ik_x x')\mathbf{V}(z'). \qquad (30)$$

Only the y component of the induced currents contributes to variations in the magnetic field near the ground surface. The y component of the induced current I_y is given by

$$I_y(z') = \sigma(z')\left[V_z(z')B_x^{amb} - V_x(z')B_z^{amb}\right]. \qquad (31)$$

For an assumed 1-D structure of conductivity, the functions $U_y^{(n)}$ and $D_y^{(n)}$ ($n = 0, \cdots, N$) in eq. (21) are determined to satisfy eqs (26) and (27). The EM field (B_x, B_z and E_y) is determined by completing the integrals of eqs (13), (15) and (17). Examples of derived expressions of the EM field are presented in Appendix B.

4 AMPLITUDES OF VARIATIONS IN THE MAGNETIC FIELD

To estimate variations in the EM field because of electric currents induced by seismic waves, the calculation must consider the structure of electrical conductivity beneath the site of interest. Conductivity structures are determined from EM soundings. However, it is frequently laborious to accurately determine conductivity in the deep crust, particularly if the upper crust is relatively conductive. It is therefore important to explore how uncertainty regarding conductivity affects calculated variations in the EM field. It is also important to identify quantities that do not depend on details of conductivity structure, if such quantities exist.

Below, numerical examples are presented of the amplitudes of variations in the magnetic field ($|B_i|$; $i = x$ or z) arising from ground motions produced by Rayleigh waves. Because surface waves are dominant at a significant distance from the epicentre, and because Love waves do not generate variations in the magnetic field (as verified above), it is reasonable to focus on Rayleigh waves. Each component of ground motions corresponding to Rayleigh waves is expressed as

$$V_x(x', z') = -\omega A_R \exp(ik_x x')$$
$$\times \left[\exp\left(-v_R\eta_P k_x z'\right) + \frac{1}{2}\left(\frac{v_R^2}{v_S^2} - 2\right)\exp(-v_R\eta_S k_x z')\right], \qquad (32)$$

$$V_z(x', z') = +i\omega A_R \exp(ik_x x')$$
$$\times \left[v_R\eta_P \exp(-v_R\eta_P k_x z')\right.$$
$$\left. + \frac{1}{2v_R\eta_S}\left(\frac{v_R^2}{v_S^2} - 2\right)\exp(-v_R\eta_S k_x z')\right], \qquad (33)$$

and $V_y(x', z') = 0$, where A_R and $k_x = \omega/v_R = 2\pi/(v_R T)$ represent the amplitude in displacement and the wavenumber, respectively; T is the period; v_P, v_S and v_R represent the velocities of the P, S and Rayleigh waves, respectively; and η_P and η_S represent $(v_R^{-2} - v_P^{-2})^{1/2}$

Table 1. Values of parameters adopted in numerical tests.

Parameter	Value
x component of the ambient geomagnetic field (B_x^{amb})	35 000 nT
z component of the ambient geomagnetic field (B_z^{amb})	35 000 nT
P-wave velocity (v_P)	6.0 km s^{-1}
Amplitude of displacement of the Rayleigh wave (A_R)	0.01 m
Geomagnetic observation altitude (z)	0 m
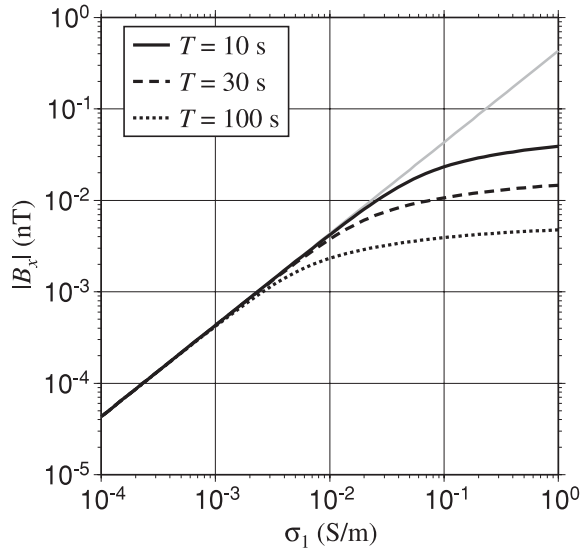
Figure 2. Amplitudes of variations in the magnetic field ($|B_x|$) because of Rayleigh waves, plotted against conductivity of the lower half-space (σ_1). Solid, broken and dotted curves in black represent the results for frequencies ($T = 2\pi/\omega$) of 10, 30 and 100 s, respectively. The grey line represents the amplitudes estimated by the Biot–Savart law, which is equivalent to ignoring conductive currents. Note that the magnitudes of variations in the magnetic field are invariant to the frequency; therefore, there is only one line in grey.

and $(v_R^{-2} - v_S^{-2})^{1/2}$, respectively (e.g. Lay & Wallace 1995). Herein, a Poisson solid is assumed, for which v_R/v_P and v_S/v_P take values of 0.531 and 0.577, respectively.

Table 1 lists the parameters employed in the following examples. Amplitudes of displacement, velocity and acceleration of the Rayleigh wave are given by A_R, ωA_R and $\omega^2 A_R$, respectively. The results are normalized to $A_R = 1$ cm. Because results are simply proportional to A_R, the results for other values of A_R are obtained by multiplying by an appropriate factor.

First, consider a two-layer model comprising an upper half-space of resistive air ($\sigma = \sigma_0 = 0$) and a lower half-space of crust with uniform conductivity ($\sigma = \sigma_1$). In two- and three-layer models, $|B_x| = |B_z|$ is satisfied in the upper half-space (see APPENDIX B); therefore, it is sufficient to consider only $|B_x|$. Fig. 2 shows examples of the estimated $|B_x|$.

A striking feature is a monotonic increase in $|B_x|$ with increasing conductivity for a given period of seismic waves ($T = 2\pi/\omega$). Note that this result is not trivial. The intensity of the source currents ($\mathbf{I}^i$ in eq. 7) is proportional to the conductivity of the crust (σ_1). Consequently, it may seem logical that high conductivity would result in large EM variations. However, high conductivity also acts to attenuate EM variations propagating from lower points of the crust, because of the skin effect. In fact, $|B_x|$ is not strictly proportional to the crust's conductivity (σ_1). For example, see the case of $T = 30$ s (dashed lines in Fig. 2) and compare with $|B_x|$s corresponding

to $\sigma_1 = 1$ and 0.01 S m^{-1}. The expected $|B_x|$ corresponding to the former case is only three times larger than that in the latter case, despite the large difference in conductivity (by a factor of 100). In all cases of $T = 10$, 30 and 100 s, $|B_x|$ for high conductivity is strongly suppressed to certain upper limits according to the frequencies of the corresponding seismic waves. We can rigorously confirm $|B_x|$ has an asymptotic limit as σ_1 approaches infinity, and the asymptotic limit is proportional to T^{-1} (see Appendix B3). Nevertheless, $|B_x|$ shows a monotonic increase as a function of σ_1 over the range of conductivities considered here.

The results obtained for the two-layer model indicate that we cannot calculate variations in the magnetic field arising from the motional induction in the framework of magnetostatics, although some earlier studies (e.g. Taira *et al*. 2009) have attempted to do so. By ignoring conductive currents, Maxwell's equations reduce to the simpler Biot–Savart law. However, Fig. 2 clearly shows such a simplification is not valid for large σ_1. Calculation by the Biot–Savart law provides a good approximation only when conductivity is low. In the case of $T = 30$ s, for example, $|B_x|$ values at $\sigma_1 = 0.1$ S m^{-1} calculated by the Biot–Savart law are about five times larger than the correct value. Consequently, it is concluded that Maxwell's equations are necessary for accurate estimations of $|B_x|$.

Next, consider a three-layer model comprising of an upper half-space of resistive air ($\sigma = 0$), a middle layer of upper crust ($\sigma = \sigma_1$), and a lower half-space of deep crust ($\sigma = \sigma_2$). Because the energy of Rayleigh waves is concentrated near the Earth's surface and decays exponentially with increasing depth, the effect of induced currents should also decay with increasing depth in generating variations in the EM field at the ground surface. Therefore, it is reasonable to test whether the amplitudes of variations in the magnetic field are approximately independent of conductivity in the deep crust.

Numerical examples show however that conductivity in the deep crust may have a strong effect on the generated $|B_x|$. For example, consider the case of $T = 30$ s and $z_1 = 5$ km (Fig. 3a). Compared with the three-layer model with $\sigma_2 = 0.01$ S m^{-1}, the two-layer model predicts a considerably small value of $|B_x|$ when $\sigma_1 < 0.01$ S m^{-1}, and a somewhat large value when $\sigma_1 > 0.01$ S m^{-1}, except for extremely large σ_1. The same trends are seen for other values of σ_2 and other depths of the boundary (Fig. 3b). These examples show that incorrect values of conductivity for the deep crust can lead to incorrect estimations of the induced variations in the EM field. The same conclusions are derived for seismic waves with other periods ($T = 10$ and 100 s), although numerical examples are not shown here.

Nevertheless, the two-layer model provides an upper limit to possible amplitudes of variations in the magnetic field generated by induced currents. The results in Fig. 3 suggest that $|B_x|$ values arising from the three-layer model are generally smaller than those predicted by the two-layer model assuming a conductivity of the crust to be the maximum of σ_1 and σ_2. Given that $|B_x|$ is approximately a monotonically increasing function of σ_1 and σ_2, it is anticipated that this result would hold for N-layered (where $N \geq 2$) cases. A two-layer model, assuming the conductivity of the crust to be the maximum of σ_n ($0 < n < N$) provides the upper limit of the possible values of $|B_x|$.

Based on the above discussion, an upper limit of $|B_i|$ is roughly obtained using a two-layer model assuming a high conductivity (e.g. 0.1 S m^{-1}). An important conclusion is that the expected amplitudes of variations in the magnetic field are small. For example, the maximum $|B_x|$ corresponding to $T = 30$ s and $A = 1$ cm is only 0.01 nT. Even if the displacement amplitude of the Rayleigh wave is $A_R = 10$

(a) $z_1 = 5$ km and $T = 30$ s

(b) $z_1 = 10$ km and $T = 30$ s
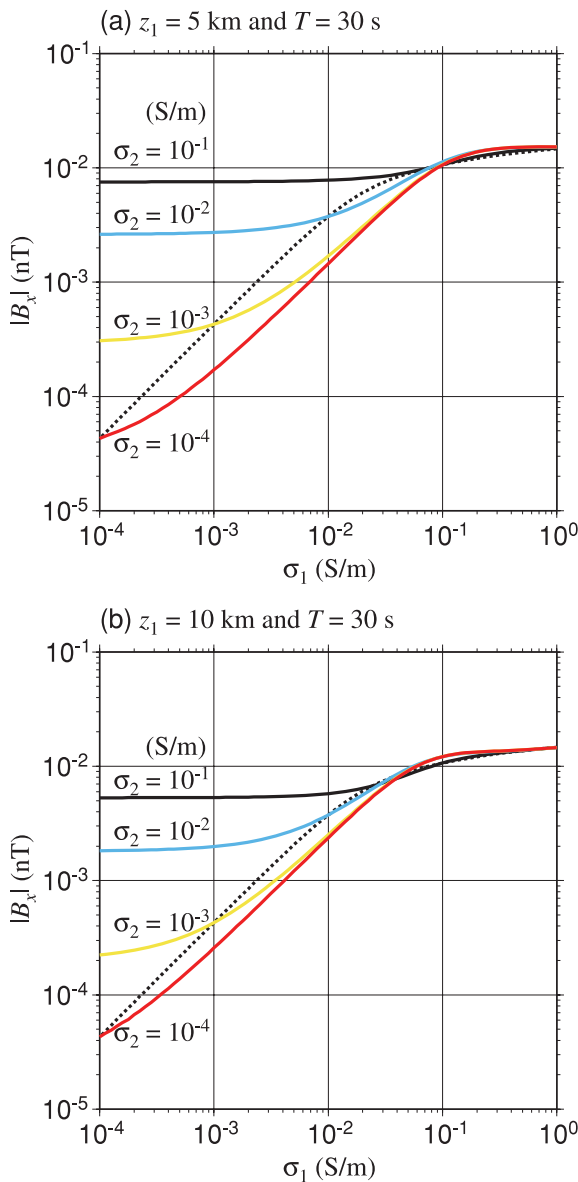
Figure 3. Amplitudes of variations in *x*-component of the magnetic field ($|B_x|$) because of Rayleigh waves, plotted against the conductivity of the upper crust (σ_1) for a conductivity boundary at a depth of (a) 5 km and (b) 10 km. Results are shown for different values of conductivity in the lower half-space (σ_2), and when assuming $\sigma_1 = \sigma_2$ (dotted curves).

cm, the expected $|B_x|$ is only 0.1 nT. This value is close to the limit of detection by conventional instruments, including fluxgate magnetometers under typical observation conditions (e.g. Turner *et al.* 2007). If variations in the magnetic field with notable amplitudes (>0.1 nT) are observed, they are not interpreted to be arisen from the motional induction.

Future advances in data processing techniques may enable the detection of variations in the magnetic field induced by seismic waves with an accuracy of 0.01 nT. This possibility provides the motivation to obtain more precise estimates of $|B_i|$ to establish theoretical predictions for comparison to future observations. If the observed $|B_i|$ is much smaller than the calculated upper limit, and if other possibilities (e.g. the electrokinetic effect and external disturbances) can be excluded, then it is tentatively concluded the existence of resistive layers beneath conductive layers in the upper crust.

5 PHASES OF VARIATIONS IN THE MAGNETIC FIELD

It is useful to investigate the characteristics of the phase of magnetic field variations arising from motional induction, because this may help to distinguish signals arising from motional induction from those resulting from other mechanisms.

An important feature of the magnetic field variations arising from the motional induction is the difference in the phases of B_x and B_z, which is apparent from eqs (13) and (15), respectively. Expression (13) is obtained by replacing $\partial/\partial z$ in expression (15) with $-ik$. The operator $\partial/\partial z$ acts on the function G_i expressed by eq. (21). Now consider the case in which the observation point z is located in the air layer. In this layer (i.e. $n = 0$), the second and third terms in eq. (21) become zero, and $u_n = |k|$. Given that the Rayleigh waves propagate in the positive x direction, we have $u_n = k$. In this case, the operator $\partial/\partial z$ acting on G_i is equivalent to multiplying k. Consequently, it is concluded that B_z is obtained by multiplying B_x by $-i$. In other words, the phase of B_z precedes that of B_x by 90°.

The difference between the phases of B_x and ground motions cannot be analytically derived; thus, numerical simulations are required. A three-layer model is assumed with the same parameters as in the previous section. Fig. 4 shows two sets of results corresponding to layers boundaries (z_1) of different depths.

If we focus only on conductivity values for which high amplitudes of $|B_x|$ are expected (>0.01 nT), we find a narrow range of phase difference (30°–80°). A similar feature is observed for other values of T and v_R, although numerical examples are not shown here.

The range of phase differences is roughly interpreted as follows. Directions of particle motions of Rayleigh waves depend on depth (e.g. see fig. 5.11 of Aki & Richards 2002). While particle motion at the ground surface is anticlockwise, particle motion at a deeper level is clockwise. Consequently, the phases of induced currents I_y at deeper levels should be different from those at the ground surface. Because **B** is generated from the sum of contributions from each depth, it is natural that the range of phase difference between V_x and B_x would be large. However, when the conductivity is high, the contributions from deeper levels are strongly attenuated. In the case that contributions from deeper levels in the crust are strongly attenuated, the phase of B_x is determined mainly by the phase of I_y at shallower levels. As shown in the previous section, high conductivity is necessary to generate B_x with a high amplitude. Consequently, the phases of B_x with high amplitude are determined mainly by the phase of I_y at shallow levels in the crust. This explains why the phase difference falls within a relatively narrow range when $|B_x|$ is large.

The quantitative aspects of the results shown in Fig. 4 should be modified when the direction of $\mathbf{B}^{amb}$ changes. The x direction is that of Rayleigh wave propagation. Phase differences depend on the assumed geometry of wave propagation and the ambient geomagnetic field. However, as long as the conductivity has a layered structure, qualitative aspects of the above discussion remain valid even if the geometry is changed.

The phase difference between B_x and V_x is used to distinguish magnetic variations generated by motional induction from incorrectly recorded variations because of sensor vibrations, if precise

(a) $z_1 = 5$ km and $T = 30$ s

(b) $z_1 = 10$ km and $T = 30$ s
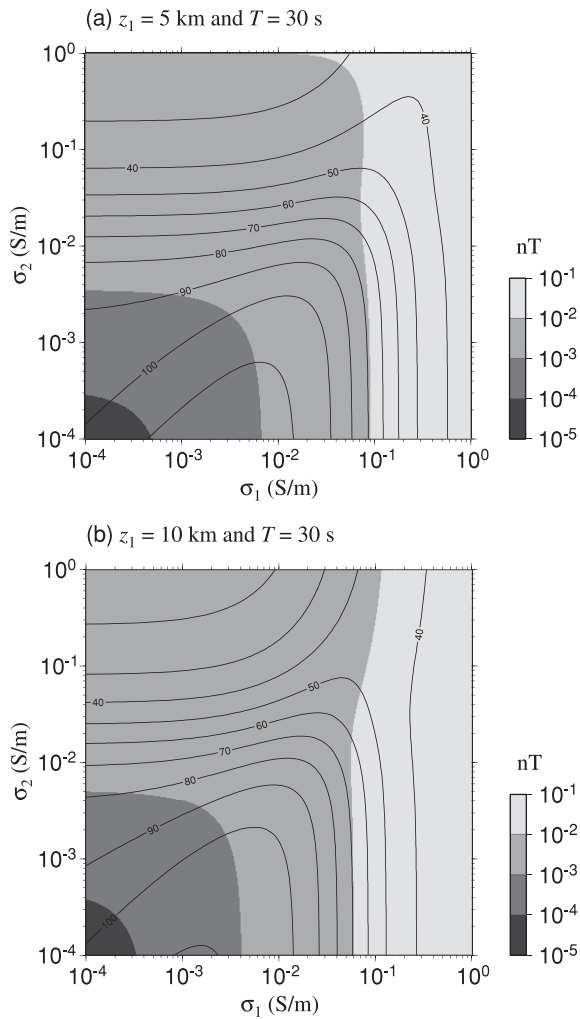
Figure 4. Phase differences between V_x and B_x (i.e. phase of V_x minus phase of B_x) for two different depths of conductivity boundary. Grey shading shows the amplitude of B_x. (a) The case of $z_1 = 5$ km. (b) The case of $z_1 = 10$ km.

ground motions are available at the site of the magnetometer. A rough prediction of the phase difference between B_x and V_x can be obtained by a simplified calculation assuming a two-layer model. If the observed phase differences are inconsistent with the predictions derived from the two-layer model, variations in the magnetic field are judged not to have arisen from the motional induction that accompanies Rayleigh waves.

6 DISCUSSION

6.1 Comparison with other mechanisms

Among several candidate mechanisms that convert seismic ground motions to EM variations, this paper has considered only motional induction up to this point. However, if this mechanism proves to be insignificant compared with other mechanisms, theoretical calculations considering motional induction would be largely meaningless in terms of comparisons with observations. Therefore, it is important to compare the amplitudes of variations in the magnetic field arising from motional induction, with the amplitudes arising from other mechanisms.

In fluid-saturated porous media, the most important mechanism that converts seismic waves to EM variations is generally considered to be the electrokinetic effect (e.g. Gao & Hu 2010, and references therein). Although the intensity of the current induced by the electrokinetic effect is strongly dependent on parameters including permeabilities of materials (e.g. Jouniaux *et al*. 1994; Jouniaux & Pozzi 1995), previous numerical evaluations have demonstrated that variations in the magnetic field caused by the electrokinetic effect may be much larger than those generated by the motional induction (e.g. Gershenzon & Bambakidis 2001).

However, it is important to consider the differences in this study (surface waves are dominant) and in previous studies (body waves are dominant). An important difference between body waves and surface waves is that the dominant frequencies of body waves are much higher. Consequently, EM variations generated by the motional induction that accompanies body waves are strongly attenuated because of the skin effect. EM variations generated by the electrokinetic effect are also strongly attenuated in the case of body waves. However, the electrokinetic effect is significant only in a rather thin (i.e. up to several metres) layer near the ground surface. Consequently, the attenuation of EM variations is rather week for signals of electrokinetic origin. This explains why the electrokinetic effect is more important than the motional induction in generating EM variations associated with body waves. In the case of surface waves, the motional induction is not necessarily insignificant compared with the electrokinetic effect.

It is also important to note that the electrokinetic effect can convert *SH* seismic waves into variations in the EM field (Garambois & Dietrich 2001), even if the seismic waves are assumed to be plane waves. Indeed, in the assumed situation (i.e. plane seismic waves in the Earth with a layered structure), only the y components of ground motions are converted to EM variations by the electrokinetic effect. This prediction can be confirmed as follows. In Section 3, it is shown that only the y components of electric currents (i.e. I_y) contribute to EM variations on the ground. For the motional induction, I_y is induced only by the x or z components of ground motions; thus, only P and SV waves contribute to the generation of EM variations. In contrast, for the electrokinetic effect, I_y is induced only by the y components of ground motions; thus, in that case, only *SH* waves can contribute to the generation of EM variations.

The piezomagnetic effect (i.e. changes in magnetization under the application of mechanical stress) is also a possible mechanism that converts mechanical forces into EM variations. Yamazaki (2011a) derived a set of analytical expressions of the EM variations generated by the piezomagnetic effect, corresponding to the same seismic situation as in this study (i.e. plane waves propagating within a layered conductivity structure). The amplitude of the piezomagnetic signal is estimated to be approximately 0.03 nT (see fig. 3 in Yamazaki 2011a). However, this estimation was obtained by assuming extremely large magnetizations of the crust (~ 7.0 A m^{-1}). For typical values of magnetization (i.e. <1.0 A m^{-1}), piezomagnetic signals are much smaller than those generated by the motional induction in conductive crust. The piezomagnetic effect may be dominant when the observation site is located near a strong (~ 10 A m^{-1}) magnetization boundary (Yamazaki 2011b), but such strong boundaries (e.g. Nishida *et al*. 2004) are an extreme case.

6.2 Future perspectives

When we attempt to compare actual and theoretical variations in the magnetic field, it is necessary to consider the possibility that

variations in vector magnetic field data are caused by sensor vibrations. To assess whether known theories explain observations, based on a comparison between data and theoretical predictions, it is necessary to exclude the possibility of sensor vibrations or to establish a methodology of correcting such vibrations.

A practical option is to examine seismograms. If a precise seismogram is available, it would be possible to identify and thereby remove distortion of the geomagnetic data arising from vibrations of the vector magnetometer. For this purpose, the seismometer should be installed at the same site as the corresponding magnetometer. Because seismic ground motions are highly site dependent, seismograms at a remote station may provide erroneous predictions of ground motions at the location of the magnetometer. Given that seismometers and magnetometers are rarely installed at the same location, it would be necessary to set up suitable observation stations if we are to adopt this strategy.

Another approach that would enable a comparison between data and theory would be to focus on variations in the magnetic field before the arrival of seismic waves. When a pulse of seismic waves approaches a site, EM variations converted from the waves are expected to occur before their arrival (Gershenzon *et al*. 1994). Geomagnetic time-series for the period before the arrival of seismic waves are not distorted by the seismic ground motions; therefore, vector geomagnetic data can be compared with theory without considering the possibility of sensor vibrations. The main challenge in employing this strategy is the small magnitude of the expected signals. Because magnetic variations that occur before seismic waves should be much smaller than those simultaneous with seismic waves, this approach requires further advances in sensor and data-processing technologies.

7 CONCLUSIONS

For situations in which the conductivity of the Earth's crust has a layered structure and seismic waves are expressed as plane waves, analytical expressions can be developed for variations in the EM field arising from the motional induction that accompanies seismic waves. In this situation, ground motions corresponding to *SH* waves, including Love waves, do not generate variations in the EM field above the ground surface. The amplitudes of the generated variations in the magnetic field show a monotonic increase with increasing conductivity. Attenuation because of the skin effect of the conductive crust should be incorporated into the estimation; otherwise, the amplitudes of variations in the magnetic field will be significantly overestimated. The amplitude of the generated magnetic field may be sensitive to conductivity in both the shallow and deep crust, thereby introducing errors into the calculation. Nevertheless, calculations assuming a simplified structure of conductivity provide an upper limit to the possible variations in the magnetic field because of seismic waves. For example, the amplitudes of variations in the magnetic field arising from a Rayleigh wave with a displace amplitude of 10 cm and a period of 30 s are estimated to be up to 0.1 nT, which is close to the limit of detection by conventional instruments, including fluxgate magnetometers under typical observation conditions. It is also suggested that phase differences between seismic ground motions and variations in the magnetic field are not influenced by detailed conductivity structures, and that they occur within a rather narrow range of values determined by the orientation of the ambient geomagnetic field. This property may be used to distinguish variations arising from the motional induction, from

other origins when data with an accuracy of 0.01 nT are available in the future.

REFERENCES

Abdul Azeez, K.K., Manoj, C., Veeraswamy, K. & Harinarayana, T., 2009. Co-seismic EM signals in magnetotelluric measurement—a case study during Bhuj earthquake (26th January 2001), India, *Earth Planets Space,* **61,** 973–981.

Aki, K. & Richards, P.G., 2002. *Quantitative Seismology,* 2nd edn, University Science Books, Sausalito, CA, 704pp.

Bishop, J.R., 1981. Piezoelectric effects in quartz-rich rocks, *Tectonophysics,* **77,** 297–321, doi:10.1016/0040-1951(81)90268-7.

Bordes, C., Jouniaux, L., Dietrich, M., Pozzi, J.-P. & Garambois, S., 2006. First laboratory measurements of seismo-magnetic conversions in fluid-filled Fontainebleau sand, *Geophys. Res. Lett.,* **33,** L01302, doi:10.1029/2005GL024582.

Bordes, C., Jouniaux, L., Garambois, S., Dietrich, M., Pozzi, J.P. & Gaffet, S., 2008. Evidence of the theoretically predicted seismo-magnetic conversion, *Geophys. J. Int.,* **174,** 489–504, doi:10.1111/j.1365-246X.2008.03828.x.

Eleman, F., 1965. The response of magnetic instrument to earthquake waves, *J. Geomag. Geoelectr.,* **18,** 43–72.

Gao, Y. & Hu, H., 2010. Seismoelectromagnetic waves radiated by a double couple source in a saturated porous medium, *Geophys. J. Int.,* **181,** 873–896, doi:10.1111/j.1365-246X.2010.04526.x.

Garambois, S. & Dietrich, M., 2001. Seismoelectric wave conversions in porous media: Field measurements and transfer function analysis, *Geophysics,* **66,** 1417–1430.

Garambois, S. & Dietrich, M., 2002. Full waveform numerical simulations of seismoelectromagnetic wave conversions in fluidsaturated stratified porous media, *J. geophys. Res.,* **107**(B7), 2148, doi:10.1029/2001JB00316.

Gershenzon, N.I., Gokhberg, M.B. & Yunga, S.L., 1993. On the electromagnetic field of an earthquake focus, *Phys. Earth planet. Inter.,* **77,** 13–19, doi:10.1016/0031-9201(93)90030-D.

Gershenzon, N.I. & Bambakidis, G., 2001. Modeling of seismo-electromagnetic phenomena, *Russ. J. Earth Sci.,* **3**(4), 247–275.

Gershenzon, N.I., Gokhberg, M.B. & Gul'yel'mi, A.V., 1994. Electromagnetic field of seismic pulses, *Phys. Solid Earth,* **29**(9), 789–194.

Ghomshei, M.M. & Templeton, T.L., 1989. Piezoelectric and *a*-axes fabric along a quartz vein, *Phys. Earth planet. Inter.,* **55,** 374–386, doi:10.1016/0031-9201(89)90084-8.

Haartsen, M.W. & Pride, S.R., 1997. Electroseismic waves from point sources in layered media, *J. geophys. Res.,* **102,** 24 745–24 769, doi:10.1029/97JB02936.

Honkura, Y., Matsushima, M., Oshiman, N., Tunçer, M.K., Baris, S., Ito, A. & Iio, Y., 2002. Small electric and magnetic signals observed before the arrival of seismic wave, *Earth Planets Space,* **54,** e9–e12.

Honkura, Y., Satoh, H. & Ujihara, N., 2004. Seismic dynamo effects associated with the M7.0 earthquake of 26 May 2003 off Miyagi Prefecture and the M6.2 earthquake in northern Miyagi Prefecture, NE Japan, *Earth Planets Space,* **56,** 109–114.

Honkura, Y., Ogawa, Y., Matsushima, M., Nagaoka, S., Ujihara, N. & Yamawaki, T., 2009. A model for observed circular polarized electric fields coincident with the passage of large seismic waves, *J. geophys. Res.,* **114,** B10103, doi:10.1029/2008JB006117.

Huang, Q., 2002. One possible generation mechanism of co-seismic electric signals, *Proc. Japan. Acad.,* **78**(B7), 173–178, doi:10.2183/pjab.78.173.

Ishido, T. & Mizutani, H., 1981. Experimental and theoretical basis of electrokinetic phenomena in rock-water systems and its application to geophysics, *J. geophys. Res.,* **86,** 1763–1775, doi:10.1029/JB086iB03p01763.

Jouniaux, L., Lallemant, S. & Pozzi, J., 1994. Changes in the permeability, streaming potential and resistivity of a claystone from the Nankai prism under stress, *Geophys. Res. Lett.,* **21,** 149–152.

Jouniaux, L. & Pozzi, J.-P., 1995. Permeability dependence of streaming potential in rocks for various fluid conductivities, *Geophys. Res. Lett.,* **22,** 485–488.

Karakelian, D., Beroza, G.C., Klemperer, S.L. & Fraser-Smith, A.C., 2002. Analysis of ultralow-frequency electromagnetic field measurements associated with the 1999 *M* 7.1 Hector Mine, California, Earthquake Sequence, *Bull. seism. Soc. Am.,* **92,** 1513–1524, doi:10.1785/0120000919.

Kuriki, M., Matsushima, M., Ogawa, Y. & Honkura, Y., 2011. Spectral peaks in electric field at resonance frequencies for seismically excited motion of ions in the Earth's magnetic field, *Earth Planets Space,* **63,** 503–507, doi:10.5047/eps.2011.03.010.

Lay, T. & Wallace, T.C., 1995. *Modern Global Seismology,* Academic Press, San Diego, CA, 521pp.

Matsushima, M. *et al*., 2002. Seismoelecromagnetic effect associated with the Izmit earthquake and its aftershocks, *Bull. seism. Soc. Am.,* **92,** 350–360, doi:10.1785/0120000807.

Nagata, T., 1970. Basic magnetic properties of rocks under mechanical stresses, *Tectonophysics,* **9,** 167–195, doi:10.1016/0040-1951(70)-90015-6.

Nishida, Y., Sugisaki, Y., Takahashi, K., Utsugi, M. & Oshima, H., 2004. Tectonomagnetic study in the eastern part of Hokkaido, NE Japan: discrepancy between observed and calculated results, *Earth Planets Space,* **56,** 1049–1058.

Ogawa, T. & Utada, H., 2000a. Electromagnetic signals related to incidence of a teleseismic body wave into a subsurface piezoelectric body, *Earth Planets Space,* **52,** 253–260.

Ogawa, T. & Utada, H., 2000b. Coseismic piezoelectric effects due to a dislocation 1. An analytic far and early-time field solution in a homogeneous whole space, *Phys. Earth planet. Inter.,* **121,** 273–288, doi:10.1016/S0031-9201(00)00177-1.

Okubo, K., Takeuchi, N., Utsugi, M., Yumoto, K. & Sasai, Y., 2011. Direct magnetic signals from earthquake rupturing: Iwate-Miyagi earthquake of M 7.2, Japan, *Earth planet. Sci. Lett.,* **305,** 65–72, doi:10.1016/j.epsl.2011.02.042.

Pride, S.R., 1994. Governing equations for the coupled electromagnetic and acoustics of porous media, *Phys. Rev.,* **50,** 15 678–15 696, doi:10.1103/PhysRevB.50.15678.

Stacey, F.D. & Johnston, M.J.S., 1972. Theory of the piezomagnetic effect in titanomagnetite-bearing rocks, *Pure appl. Geophys.,* **97,** 146–155.

Taira, K., Iyemori, T. & Han, D., 2009. Geomagnetic variations observed at the arrival of seismic wave of Sumatra Earthquake, Society of Geomagnetism and Earth, Planetary and Space Sciences (SGEPSS) 2009 Fall meeting, 2009 September 27–30, Kanazawa, Japan, abstract A003–02.

Turner, G.M., Rasson, J.L. & Reeves, C.V., 2007. Observation and measurement techniques, in *Geomagnetism: Treatise on Geophysics,* Vol. 5 pp. 93–146, ed. Kono, M., Elsevier, Amsterdam.

Ujihara, N., Honkura, Y. & Ogawa, Y., 2004. Electric and magnetic field variations arising from the seismic dynamo effect for aftershocks of the M7.0 earthquake of 26 May 2003 off Miyagi Prefecture, NE Japan, *Earth Planets Space,* **56,** 115–124.

Wessel, P. & Smith, W.H., 1998. Improved version of the Generic Mapping Tools released, *EOS, Trans. Am. geophys. Un.,* **79,** 579, doi:10.1029/98EO00426.

Yamazaki, K., 2011a. Piezomagnetic fields arising from the propagation of teleseismic waves in magnetized crust with finite conductivity, *Geophys. J. Int.,* **184,** 626–638, doi:10.1111/j.1365-246X.2010.04883.x.

Yamazaki, K., 2011b. Enhancement of co-seismic piezomagnetic signals near the edges of magnetization anomalies in the Earth's crust, *Earth Planets Space,* **63,** 111–118, doi:10.5047/eps.2010.12.001.

Zlotnicki, J., Pozzi, J.P. & Cornet, F.H.C., 1981. Investigation on induced magnetization variations caused by triaxial stresses, *J. geophys. Res.,* **86,** 11 899–11 909, doi:10.1029/JB086iB12p11899.

APPENDIX A: DETERMINATION OF $U_y^{(n)}$ AND $D_y^{(n)}$

When the source current exists in layer m (i.e. $z_{m-1} < z' < z_m$), the boundary conditions given by eqs (26) and (27) at z_n ($n = 0, \ldots, N-1$) yield

$$u_n \exp(+u_n z_n)\sigma_n' U_y^{(n)}(z') - u_n \exp(-u_n z_n)\sigma_n' D_y^{(n)}(z')$$
$$-u_{n+1}\exp(+u_{n+1}z_n)\sigma_{n+1}' U_y^{(n+1)}(z') + u_{n+1}\exp(-u_{n+1}z_n)\sigma_{n+1}'$$
$$\times D_y^{(n+1)}(z') = \delta_{n,m}\frac{1}{2}\exp(-u_m z_n)\exp(+u_m z')$$
$$+\delta_{n+1,m}\frac{1}{2}\exp(+u_m z_n)\exp(-u_m z'), \qquad (A1)$$

and

$$\exp(+u_n z_n)\sigma_n' U_y^{(n)} + \exp(-u_n z_n)\sigma_n' D_y^{(n)}$$
$$-\exp(+u_{n+1}z_n)\sigma_{n+1}' U_y^{(n+1)} - \exp(-u_{n+1}z_n)\sigma_{n+1}' D_y^{(n+1)}$$
$$=-\delta_{n,m}\frac{1}{2u_m}\exp(-u_m z_n)\exp(+u_m z')$$
$$+\delta_{n+1,m}\frac{1}{2u_m}\exp(+u_m z_n)\exp(-u_m z'), \qquad (A2)$$

respectively. Expressions of $\sigma_n' U_y^{(n)}(z')$ and $\sigma_n' D_y^{(n)}(z')$ are obtained by solving (A1) and (A2) for $0 \le n < N$, together with the condition of $U_y^{(N)} = D_y^{(0)} = 0$. Note that we do not need to consider the case of $m = 0$ (i.e. $z' < 0$), because no electric current exist above the ground surface ($z = 0$). Examples for two- and three-layer models ($N = 1$ and 2, respectively) are presented as follows.

A1 Two-layer model ($N = 1$)

$$\sigma_0' U_y^{(0)}(z') = \frac{1}{u_0 + u_1}\exp(-u_1 z'), \qquad (A3)$$

$$\sigma_0' D_y^{(1)}(z') = -\frac{u_0 - u_1}{2u_1(u_0 + u_1)}\exp(-u_1 z'). \qquad (A4)$$

A2 Three-layer model ($N = 2$)

The functions $\sigma_n' U_y^{(n)}(z')$ and $\sigma_n' D_y^{(n)}(z')$ for $z_{m-1} < z' < z_m$ ($m = 1, 2; z_2 = \infty$) of the three-layer model are expressed in the forms of

$$\sigma_n' U_y^{(n)}(z') = U_{n,m}^+ \exp(+u_m z') + U_{n,m}^- \exp(-u_m z') \ (n = 0 \text{ or } 1) \qquad (A5)$$

and

$$\sigma_n' D_y^{(n)}(z') = D_{n,m}^+ \exp(+u_m z') + D_{n,m}^- \exp(-u_m z') \ (n = 1 \text{ or } 2), \qquad (A6)$$

where the coefficients $U_{n,m}^{\pm}$ and $D_{n,m}^{\pm}$ are independent of z'. Explicit forms of $U_{n,m}^{\pm}$ and $D_{n,m}^{\pm}$ are presented below.

$n = 0$:

$$\begin{cases} U_{0,1}^{+} = \dfrac{1}{P}(u_1 - u_2)\exp(-u_1 z_1) \\[2mm] U_{0,1}^{-} = \dfrac{1}{P}(u_1 + u_2)\exp(+u_1 z_1) \\[2mm] U_{0,2}^{+} = 0 \\[2mm] U_{0,2}^{-} = \dfrac{2u_1}{P}\exp(+u_2 z_1), \end{cases} \qquad (A7)$$

$n = 1$:

$$\begin{cases} U_{1,1}^{+} = \dfrac{1}{2u_1 P}(u_0 + u_1)(u_1 - u_2)\exp(-u_1 z_1) \\[2mm] U_{1,1}^{-} = -\dfrac{1}{2u_1 P}(u_0 - u_1)(u_1 - u_2)\exp(-u_1 z_1) \\[2mm] D_{1,1}^{+} = -\dfrac{1}{2u_1 P}(u_0 - u_1)(u_1 - u_2)\exp(-u_1 z_1) \\[2mm] D_{1,1}^{-} = -\dfrac{1}{2u_1 P}(u_0 - u_1)(u_1 + u_2)\exp(+u_1 z_1) \\[2mm] U_{1,2}^{+} = 0 \\[2mm] U_{1,2}^{-} = \dfrac{1}{P}(u_0 + u_1)\exp(+u_2 z_1) \\[2mm] D_{1,2}^{+} = 0 \\[2mm] D_{1,2}^{-} = -\dfrac{1}{P}(u_0 - u_1)\exp(+u_2 z_1), \end{cases} \qquad (A8)$$

$n = 2$:

$$\begin{cases} D_{2,1}^{+} = \dfrac{1}{P}(u_0 + u_1)\exp(+u_2 z_1) \\[2mm] D_{2,1}^{-} = -\dfrac{1}{P}(u_0 - u_1)\exp(+u_2 z_1) \\[2mm] D_{2,2}^{+} = 0 \\[2mm] D_{2,2}^{-} = -\dfrac{1}{2u_2 P}[(u_0 + u_1)(u_1 - u_2)\exp(+u_1 z_1) \\[2mm] \qquad\qquad + (u_0 - u_1)(u_1 + u_2)\exp(-u_1 z_1)]\exp(+2u_2 z_1). \end{cases} \qquad (A9)$$

where

$$P = (u_0 + u_1)(u_1 + u_2)\exp(+u_1 z_1) \\ + (u_0 - u_1)(u_1 - u_2)\exp(-u_1 z_1). \qquad (A10)$$

Note that $\sigma_n' U_y^{(n)}$ and $\sigma_n' D_y^{(n)}$ for $N > 2$ are also expressed in the forms of (A5) and (A6), but explicit forms of $U_{n,m}^{\pm}$ and $D_{n,m}^{\pm}$ are different in these cases.

APPENDIX B: EXPLICIT FORMS OF THE ELECTROMAGNETIC FIELD

We consider electric currents in the y direction whose intensities are expressed by

$$I_y(z') = \begin{cases} A\sigma_m \exp(-pz') \ (z_{m-1} < z' < z_m, \ 0 \le m \le N), \\ 0 \qquad\qquad\qquad (z' < 0), \end{cases} \qquad (B1)$$

where A and p are constants, and z_N are defined as being $+\infty$. Electric currents are expressed in these forms when the currents are induced by motional induction and the particle velocity of the ground is expressed in the form of

$$V_i(z') = V_i(0)\exp\left(-pz'\right) \ (i = x, z) \qquad (B2)$$

by taking

$$A = V_z(0)B_x^{\mathrm{amb}} - V_x(0)B_z^{\mathrm{amb}}. \qquad (B3)$$

Substituting (B1) and (B2) into eqs (13), (15) and (17), we obtain

$$B_x(z) = -\mu_0 \sigma_0' A \sum_{m=1}^{N} \int_{z_{m-1}}^{z_m} \sigma_m \frac{\partial}{\partial z} G_y(z, z')\exp(-pz')\,\mathrm{d}z', \qquad (B4)$$

$$B_z(z) = i k_x \mu_0 \sigma_0' A \sum_{m=1}^{N} \int_{z_{m-1}}^{z_m} \sigma_m G_y(z, z')\exp(-pz')\,\mathrm{d}z', \qquad (B5)$$

and

$$E_y(z) = i\omega\mu_0 \sigma_0' A \sum_{m=1}^{N} \int_{z_{m-1}}^{z_m} \sigma_m G_y(z, z')\exp(-pz')\,\mathrm{d}z', \qquad (B6)$$

respectively. To obtain analytical expressions, these expressions are further deformed by using eq. (18). For example, B_x and B_z are deformed to

$$B_x(z) = -u_0 \mu_0 A \exp(+u_0 z) \\ \times \sum_{m=1}^{N} \sigma_m \int_{z_{m-1}}^{z_m} \left(\sigma_0' U_y^0(z')\right)\exp(-pz')\mathrm{d}z', \qquad (B7)$$

$$B_z(z) = i k_x A \mu_0 \exp(+u_0 z) \sum_{m=1}^{N} \sigma_m \int_{z_{m-1}}^{z_m} \left(\sigma_0' U_y^{(0)}(z')\right)\exp(-pz')\,\mathrm{d}z', \qquad (B8)$$

for $z < 0$, and to

$$B_x(z) = -u_n \mu_0 A \exp(+u_n z) \\ \times \left[\sum_{m=1}^{N} \sigma_m \int_{z_{m-1}}^{z_m} \left(\sigma_0' U_y^{(n)}(z')\right)\exp(-pz')\,\mathrm{d}z'\right] \\ + u_n \mu_0 A \exp(-u_n z) \\ \times \left[\sum_{m=1}^{N} \sigma_m \int_{z_{m-1}}^{z_m} \left(\sigma_n' D_y^{(n)}(z')\right)\exp(-pz')\,\mathrm{d}z'\right] \\ + \frac{1}{2}\mu_0 A \sigma_n \exp(-u_n z) \int_{z_{n-1}}^{z} \exp(+u_n z')\exp(-pz')\,\mathrm{d}z' \\ - \frac{1}{2}\mu_0 A \sigma_n \exp(+u_n z) \int_{z}^{z_n} \exp(-u_n z')\exp(-pz')\,\mathrm{d}z', \qquad (B9)$$

$$B_z(z) = i k_x \mu_0 A \exp(+u_n z) \\ \times \left[\sum_{m=1}^{N} \sigma_m \int_{z_{m-1}}^{z_m} (\sigma_0' U_y^{(n)}(z'))\exp(-pz')\,\mathrm{d}z'\right] \\ + i k_x \mu_0 A \exp(-u_n z) \\ \times \left[\sum_{m=1}^{N} \sigma_m \int_{z_{m-1}}^{z_m} (\sigma_n' D_y^{(n)}(z'))\exp(-pz')\,\mathrm{d}z'\right] \\ + \frac{i k_x}{2u_n}\mu_0 A \sigma_n \exp(-u_n z) \int_{z_{n-1}}^{z} \exp(+u_n z')\exp(-pz')\,\mathrm{d}z' \\ + \frac{i k_x}{2u_n}\mu_0 A \sigma_n \exp(+u_n z) \int_{z}^{z_n} \exp(-u_n z')\exp(-pz')\,\mathrm{d}z', \qquad (B10)$$

for $z > 0$, respectively. Given that $U_y^{(n)}$ and $D_y^{(n)}$ are the sums of exponentials of z', all integrals are accomplished analytically.

The expression of Rayleigh waves (eqs 32 and 33) does not have the form of (B2). However, it is separated into two terms, each of which has the form of (B2) with $p = v_R \eta_P k_x$ or $v_R \eta_S k_x$. For each term, it is possible to apply the calculation procedure developed

above. The total amount of variation in the EM field arising from the Rayleigh waves is obtained as the sum of the contributions of the two terms.

Below, explicit forms of B_x and B_z corresponding to two- and three-layer models (i.e. $N = 1$ and 2, respectively) are presented. Based on a comparison between eqs (B6) and (B7), the non-zero component of the electric field (E_y) is obtained from B_z by replacing k_x by ω.

B1 Two-layer model ($N = 1$)

B1.1 In the upper half-space (n = 0, i.e. z < 0)

$$B_x(z) = -u_0 A \mu_0 \sigma_1 \frac{1}{(u_0 + u_1)(u_1 + p)} \exp(+u_0 z), \qquad (B11)$$

$$B_z(z) = +i k_x A \mu_0 \sigma_1 \frac{1}{(u_0 + u_1)(u_1 + p)} \exp(+u_0 z). \qquad (B12)$$

B1.2 In lower half-space (n = 0, i.e. z > 0)

$$B_x(z) = -\frac{1}{2} A \mu_0 \sigma_1 \left(\frac{u_0 - u_1}{u_0 + u_1} \frac{1}{u_1 + p} + \frac{1}{u_1 - p} \right) \exp(-u_1 z)$$
$$+ \frac{1}{2} A \mu_0 \sigma_1 \left(\frac{1}{u_1 - p} - \frac{1}{u_1 + p} \right) \exp(-p z), \qquad (B13)$$

$$B_z(z) = -\frac{i k_x}{2 u_1} A \mu_0 \sigma_1 \left(\frac{u_0 - u_1}{u_0 + u_1} \frac{1}{u_1 + p} + \frac{1}{u_1 - p} \right) \exp(-u_1 z)$$
$$+ \frac{i k_x}{2 u_1} A \mu_0 \sigma_1 \left(\frac{1}{u_1 - p} + \frac{1}{u_1 + p} \right) \exp(-p z). \qquad (B14)$$

B2 Three-layer model ($N = 2$)

A function $J^{\pm}$ is defined by

$$J^{\pm}(m; a, b) = \int_a^b \exp(\pm u_m z') \exp(-p z') \, dz'$$
$$= \frac{1}{\pm u_m - p} [\exp(\pm u_m b) \exp(-p b)$$
$$- \exp(\pm u_m a) \exp(-p a)] \qquad (B15)$$

for simplicity of expression. The coefficients $U_{n,m}^{\pm}$ and $D_{n,m}^{\pm}$, which are defined in Appendix A for the case of $N = 2$, are also used.

B2.1 In the upper half-space (n = 0, i.e. z < 0)

$$B_x(z) = -u_0 A \mu_0 [\sigma_1 U_{0,1}^+ J^+(1; 0, z_1) + \sigma_1 U_{0,1}^- J^-(1; 0, z_1)$$
$$+ \sigma_2 U_{0,2}^- J^-(2; z_1, \infty)] \exp(+u_0 z), \qquad (B16)$$

$$B_z(z) = i k_x A \mu_0 [\sigma_1 U_{0,1}^+ J^+(1; 0, z_1) + \sigma_1 U_{0,1}^- J^-(1; 0, z_1)$$
$$+ \sigma_2 U_{0,2}^- J^-(2; z_1, \infty)] \exp(+u_0 z). \qquad (B17)$$

B2.2 In the middle layer (n = 1, i.e. 0 < z < z₁)

$$B_x(z) = -u_1 A \mu_0 [\sigma_1 U_{1,1}^+ J^+(1; 0, z_1) + \sigma_1 U_{1,1}^- J^-(1; 0, z_1)$$
$$+ \sigma_2 U_{1,2}^- J^-(2; z_1, \infty)] \exp(+u_1 z)$$
$$+ u_1 A \mu_0 [\sigma_1 D_{1,1}^+ J^+(1; 0, z_1) + \sigma_1 D_{1,1}^- J^-(1; 0, z_1)$$
$$+ \sigma_2 D_{1,2}^- J^-(2; z_1, \infty)] \exp(-u_1 z) + \frac{1}{2} A \mu_0 \sigma_1$$
$$\times [J^+(1; 0, z) \exp(-u_1 z) - J^-(1; z, z_1) \exp(+u_1 z)], \qquad (B18)$$

$$B_z(z) = i k_x A \mu_0 [\sigma_1 U_{1,1}^+ J^+(1; 0, z_1) + \sigma_1 U_{1,1}^- J^-(1; 0, z_1)$$
$$+ \sigma_2 U_{1,2}^-(2; z_1, \infty)] \exp(+u_1 z) + i k_x A \mu_0$$
$$\times [\sigma_1 D_{1,1}^+ J^+(1; 0, z_1) + \sigma_1 D_{1,1}^- J^-(1; 0, z_1)$$
$$+ \sigma_2 D_{1,2}^- J^-(2; z_1, \infty)] \exp(-u_1 z) + \frac{i k_x}{2 u_1} A \mu_0 \sigma_1$$
$$\times [J^+(1; 0, z) \exp(-u_1 z) + J^-(1; z, z_1) \exp(+u_1 z)]. \qquad (B19)$$

B2.3 In the lower half-space (n = 2, i.e. z₁ < z)

$$B_x(z) = +u_2 A \mu_0 [\sigma_1 D_{2,1}^+ J^+(1; 0, z_1) + \sigma_1 D_{2,1}^- J^-(1; 0, z_1)$$
$$+ \sigma_2 D_{2,2}^- J^-(2; z_1, \infty)] \exp(-u_2 z)$$
$$+ \frac{1}{2} A \mu_0 \sigma_2 [J^+(2; z_1, z) \exp(-u_2 z)$$
$$- J^-(2; z, \infty) \exp(+u_2 z)], \qquad (B20)$$

$$B_z(z) = +i k_x A \mu_0 [\sigma_1 D_{2,1}^+ J^+(2; 0, z_1)$$
$$+ \sigma_1 D_{2,1}^- J^-(2; 0, z_1) + \sigma_2 D_{2,2}^- J^-(2; z_1, \infty)]$$
$$\times \exp(-u_2 z) + \frac{i k_x}{2 u_2} A \mu_0 \sigma_2 [J^+(2; z_1, z) \exp(-u_2 z)$$
$$+ J^-(2; z, \infty) \exp(+u_2 z)]. \qquad (B21)$$

B3 Limiting values of B_x of the two-layer model

First, we consider an asymptotic limit of B_x as $\sigma_1 \to \infty$ for fixed values of other parameters. At this limit, $|u_1| \gg |u_0|$ and $|u_1| \gg p$; therefore,

$$B_x(z) \approx -\mu_0 A \sigma_1 \frac{u_0}{u_1^2} \exp(+u_0 z) = i A \frac{k_x}{\omega} \exp(+u_0 z). \qquad (B22)$$

When the amplitude of displacement is fixed, the amplitude of velocity (i.e. A) is proportional to ω. In addition, k_x is also proportional to ω. Therefore, B_x is proportional to ω.

Next, we consider the case of σ_1 being very small. Now we consider Rayleigh waves, and p is given by $v_R \eta_P k_x$ or $v_R \eta_S k_x$ (eqs 33 and 34). The parameter v_R is on the order of 10^3, and η_P and η_S are on the order of 1. Therefore, a condition of $k_x \ll p$ is always satisfied, meaning $|u_0| \ll p$. In addition, we can approximate $u_1 \approx u_0$ when $\sigma_1 \approx \sigma_0 = 0$. Taking these inequalities into account, we obtain

$$B_x(0) \approx -\frac{1}{2} \mu_0 A p^{-1} \sigma_1, \qquad (B23)$$

meaning that B_x is proportional to σ_1 and is independent of ω at this limit. The condition of $u_1 \approx u_0$ is equivalent to $\omega \mu_0 \sigma_1 \ll k_x^2$, which is satisfied when $\sigma_1 \ll 10^{-2}$ S m^{-1} for the present parameters.